

# Photometric Variations as Small Perturbations in Aerosol Content

*I. Musat*

*Department of Meteorology  
University of Maryland  
College Park, Maryland*

*R. G. Ellingson*

*Department of Meteorology  
Florida State University  
Tallahassee, Florida*

## Abstract

The quality of profile fitting of resolved stars depends ultimately upon the accuracy with which spectral differences of the sources are retrievable within the data, because the radiation color of well-separated known sources can serve as an indicator of the origin of the optical depth variations one observes during the night.

The particularities of the whole sky imager (WSI) detector and optical system are such that the data suffer from lack of the spatial resolution required in a common astronomical observation.

We construct an empirical point spread function (PSF) produced by the optical system and detector, and fit it to the data, frame by frame. Star radiance extracted with profile fitting proves to be more accurate than that from simple aperture photometry.

A bonus of the method is the possibility to construct “flat-fields”, i.e., an average of frames with stars extracted and inter-pixel variations smoothed.

## Aperture Photometry vs. Profile Fitting

Extinction calculation from starlight measurements depends crucially on the precision of inferring the star magnitude from sampled (pixelized) images. Two main methods of star photometry (or a combination of them) are frequently used: (1) aperture photometry, and (2) profile fitting.

Aperture photometry assumes that a star brightness is exactly measured as a positive signal above the surrounding sky brightness. One chooses a number of pixels (aperture) around the known star position, and deduct from their summed intensity a mean value of the surrounding “sky” which is measured in an annulus centered on the star, but is not influenced by star’s wings. Caveat: “Evaluating the diffuse component of the observed brightness at a given position in a crowded star field is extremely difficult. There are complexities concealed within the word <<sky>>. Even the meaning of the phrase “diffuse

sky brightness” cannot be perfectly defined because different things are meant under different circumstances” (Stetson 1987).

The results of the profile fitting photometry on WSI frames: the stars in the original image (Figure 1) are fitted with an empirical PSF, a 5 parameters Gaussian obtained from fitting the profiles of visible stars brighter than 2.2mag Polaris, then subtracted in 2 passes (Figure 2). The remaining stars in the residual image are subtracted in a third pass (Figure 3).

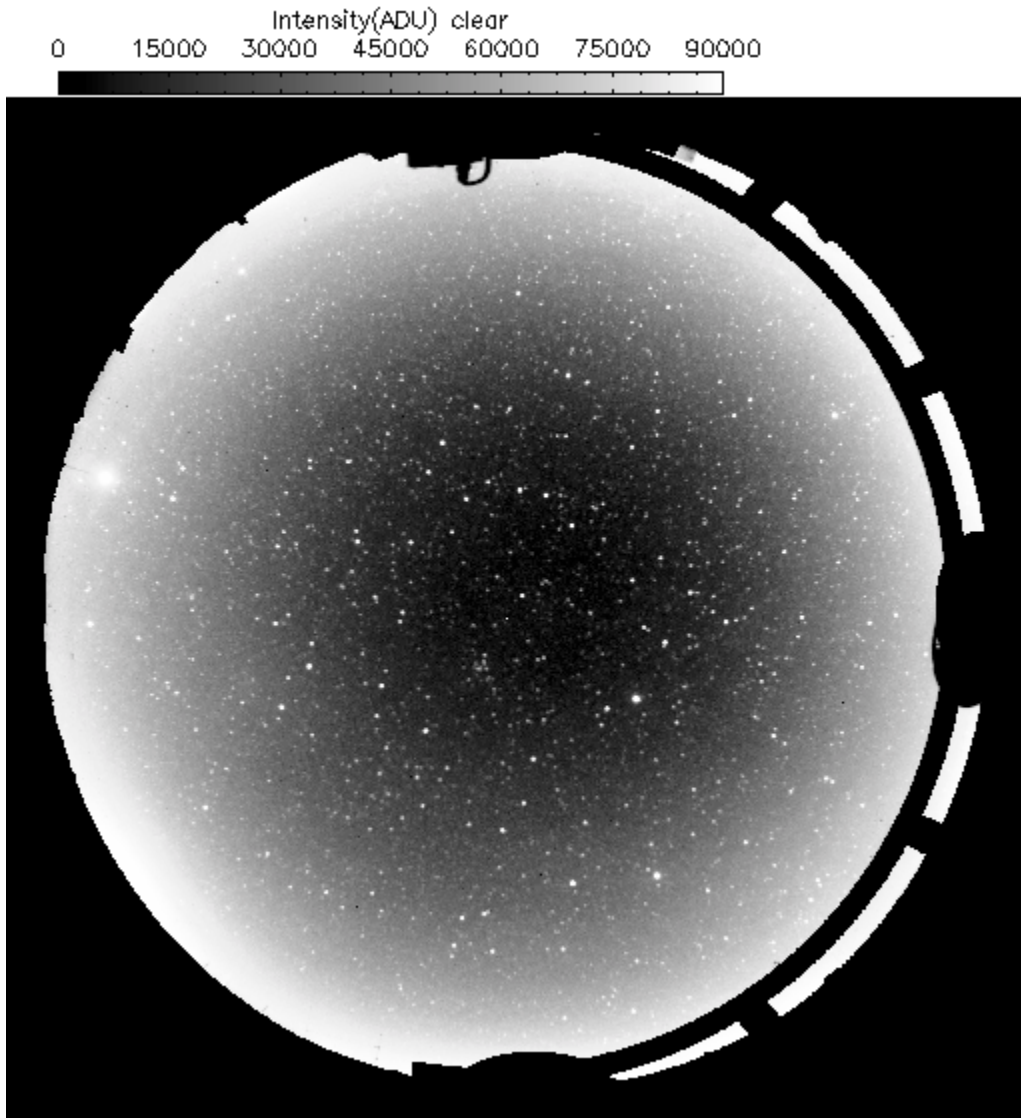


**Figure 1.** Profile fitting photometry on WSI frames: **the stars in the original image (Figure 1)** are fitted with an empirical PSF, a 5 parameters Gaussian obtained from fitting the profiles of visible stars brighter than 2.2mag Polaris, then subtracted in 2 passes (Figure 2). The remaining stars in residual image are subtracted in a third pass (Figure 3).

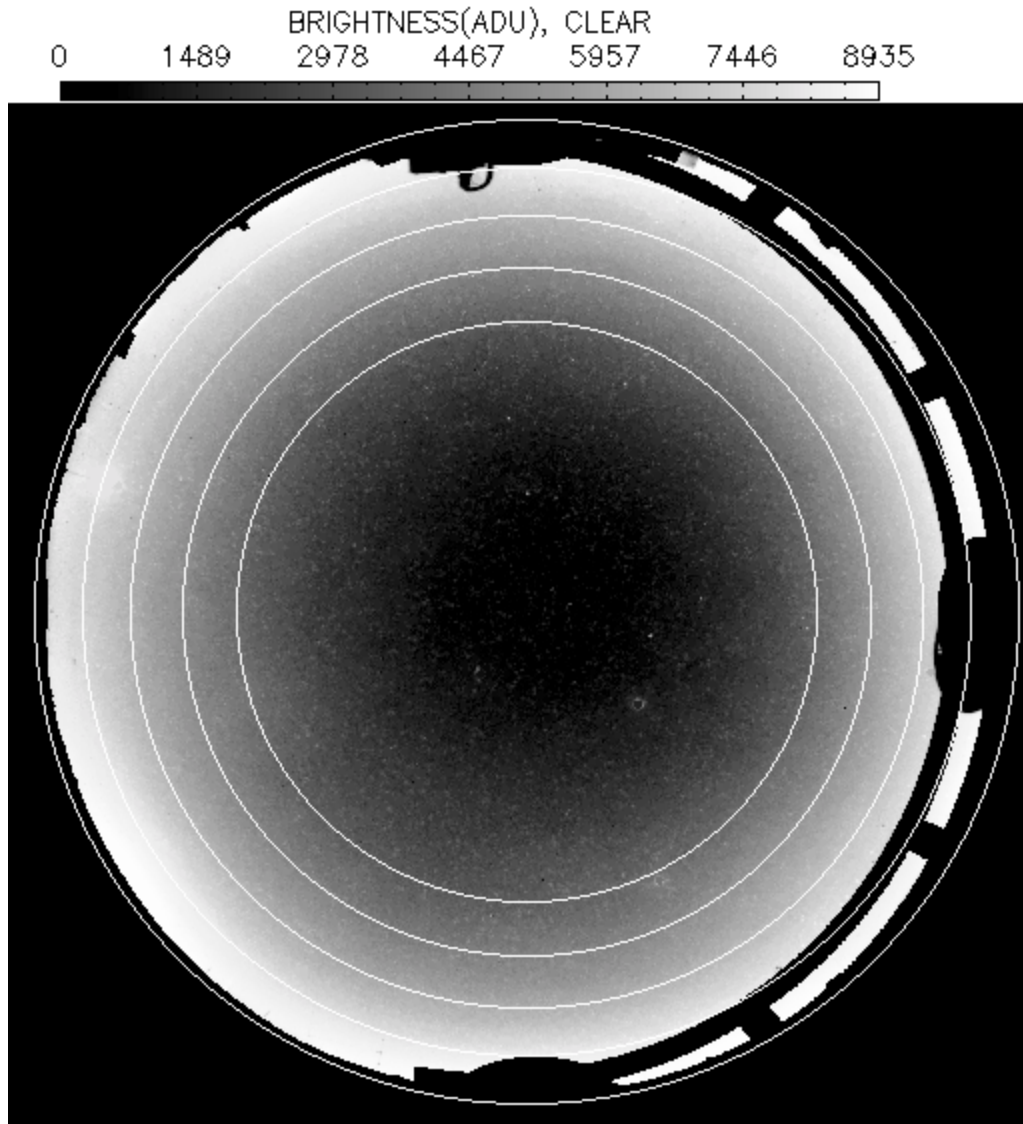


**Figure 2.** Profile fitting photometry on WSI frames: the stars in the original image (Figure 1) are fitted with an empirical PSF, a 5 parameters Gaussian obtained from fitting the profiles of visible stars brighter than 2.2mag Polaris, then subtracted in 2 passes (Figure 2). The remaining stars in residual image are subtracted in a third pass (Figure 3).

If star in the residual image is replaced by their surrounding “sky” median value, an empirical “flat” field is obtained (Figure 4). An average of well-subtracted frames should exhibit no remnants of trails (Figure 5). By contrast, too large an aperture could produce “contaminated” background sky, especially for a star with zenith larger than 60 deg., where the spatial resolution begins to drop significantly, resulting in a non-subtraction (Figure 6). The contamination with another star’s light is obvious when an elliptic aperture around a star is shown separately (Figure 7).

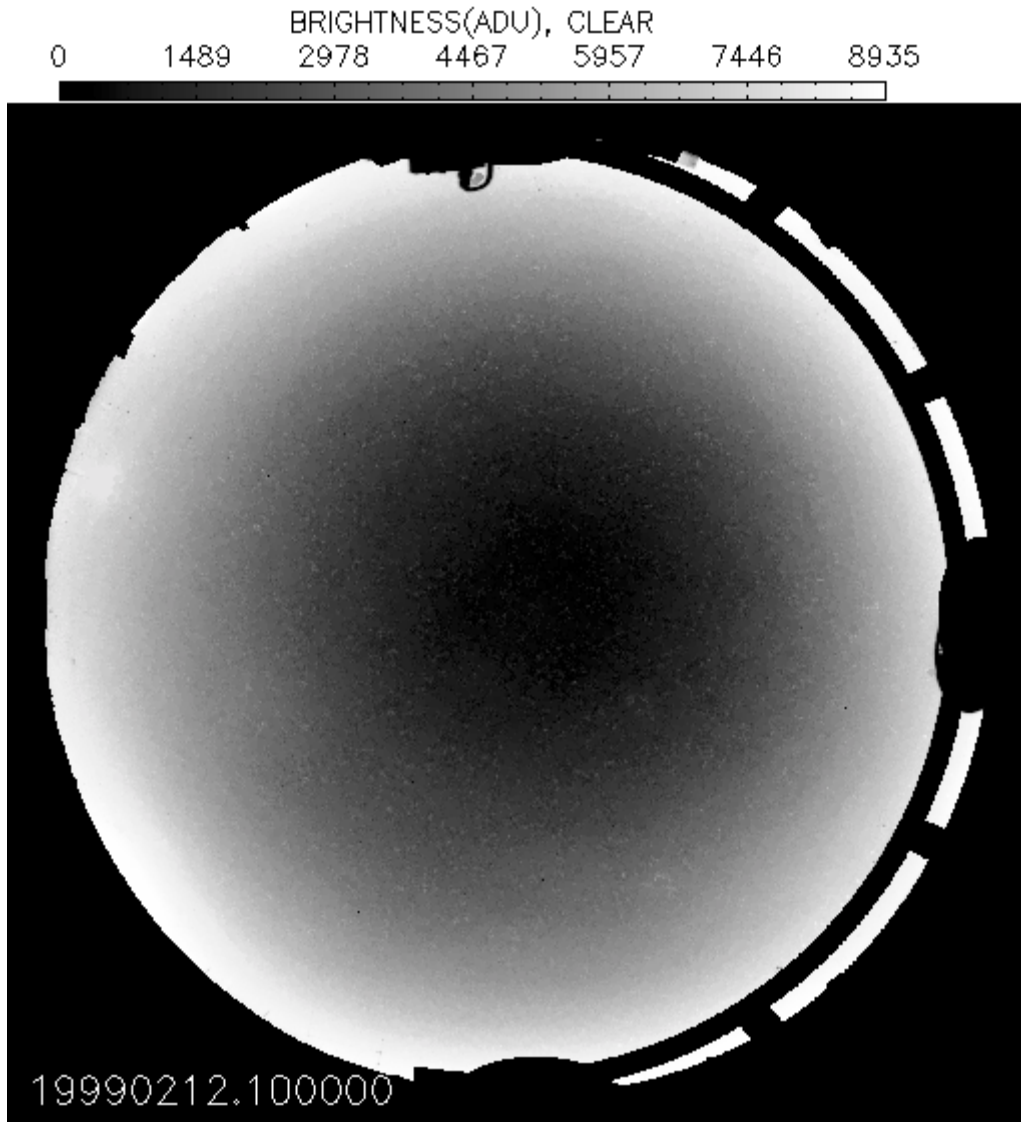


**Figure 3.** Profile fitting photometry on WSI frames: the stars in the original image (Figure 1) are fitted with an empirical PSF, a 5 parameters Gaussian obtained from fitting the profiles of visible stars brighter than 2.2mag Polaris, then subtracted in 2 passes (Figure 2). **The remaining stars in residual image are subtracted in a third pass (Figure 3).**

### Empirical PSF Construction

Profile fitting photometry assumes a model for the star image, as produced by the specifics of the detector (through pixelizing, quantum efficiency, and electronic noise), optics (modulation transfer function), “seeing” and scintillation (i.e., star position, respective, magnitude variation due to the atmospheric turbulence), differential refraction (if not monochromatic detection) etc.

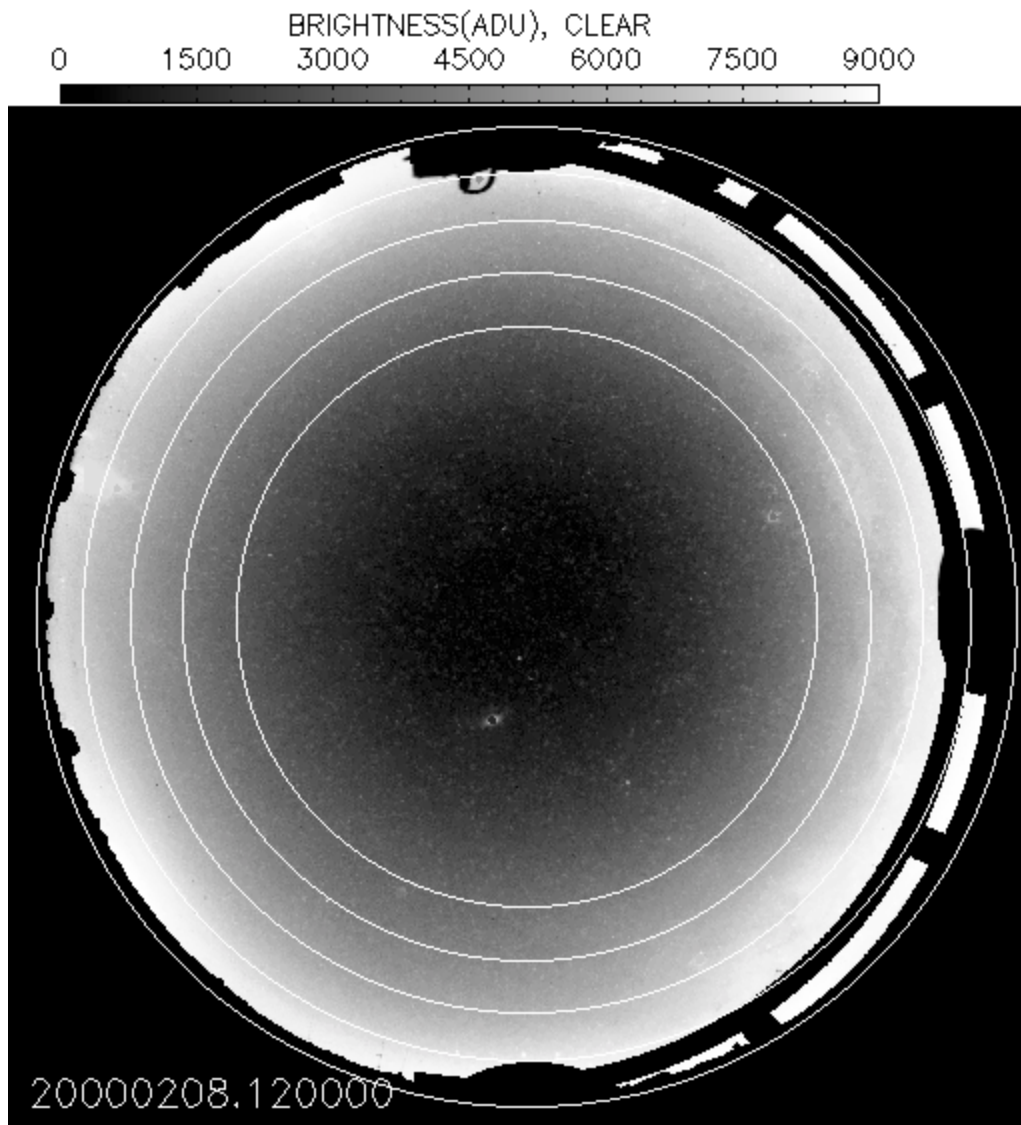


**Figure 4.** If stars in residual image are replaced by their surrounding “sky” median value, an empirical flat field is obtained (Figure 4). An average of well-subtracted frames should exhibit no remnants of trails (Figure 5). Constant zenith circles shown: 50, 60, 70, 80, 85 deg.

Fraunhofer diffraction (with the source at the infinity) of the (plane) electromagnetic monochromatic wave on a circular aperture of an optical system with aberrations produces a diffraction pattern (a Bessel function), whose shape is altered by ray and wave aberrations. For fish-eye lens the spherical aberration is overcorrected with the introduction of distortion (and magnification) for off axis rays, such that the usual “cosine to the 4th power”-drop in illumination is largely attenuated. The most important optical aberrations are defocus, distortion, and (polychromatic) lateral color shift.

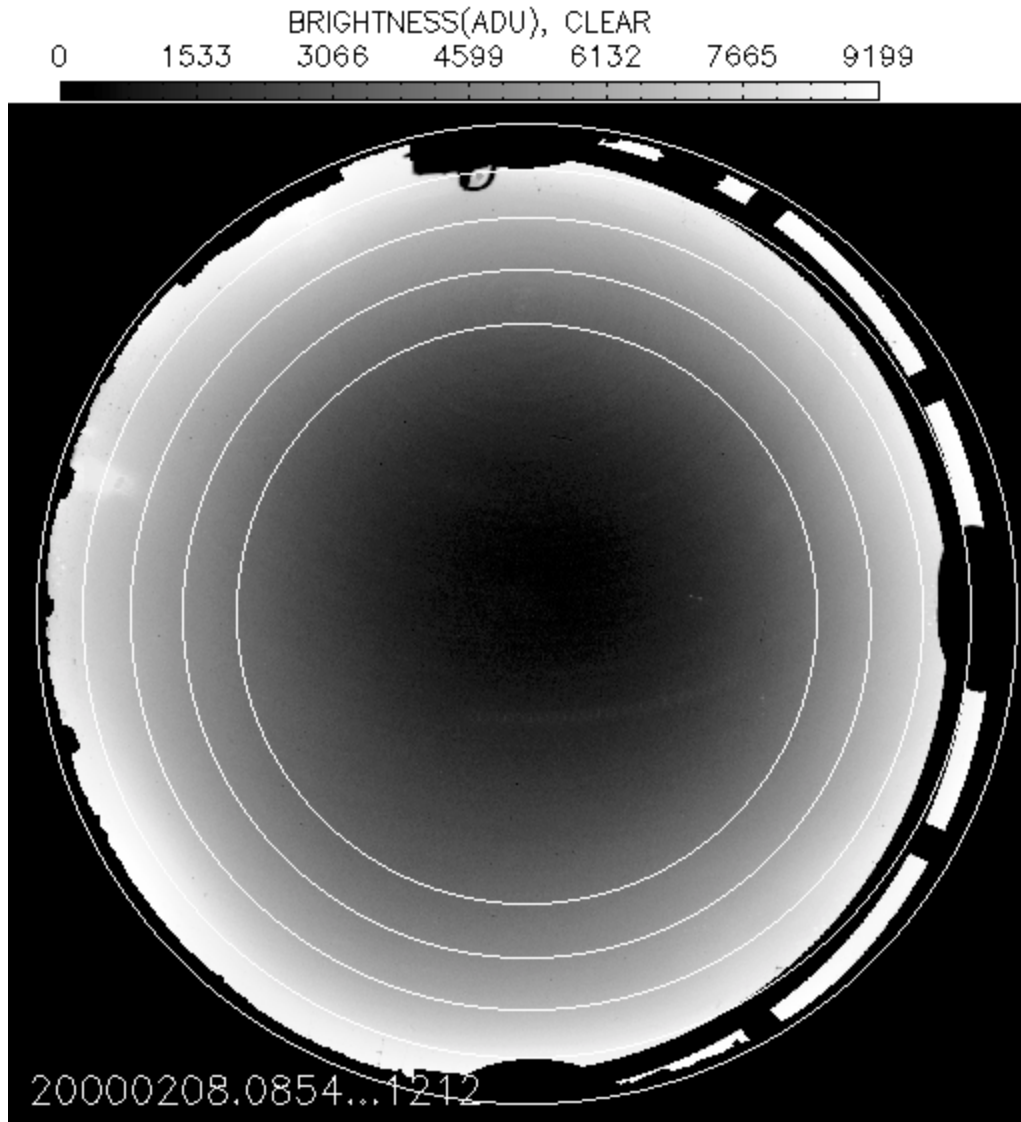


**Figure 5.** If stars in residual image are replaced by their surrounding “sky” median value, an empirical flat field is obtained (Figure 4). **An average of well-subtracted frames should exhibit no remnants of trails (Figure 5).** Constant zenith circles shown: 50, 60, 70, 80, 85 deg.

### The Point Spread Function for the Image of a Star

$$I = \text{Delta-Dirac} * \text{Optics PSF} * \text{Trail PSF} * \text{Pixel Function} + \text{Noise} = \text{PSF}$$

For broadband, the observed PSF is the result of multiple convolutions with “degrading” factors: diffraction, ray and wave aberrations, “seeing” (i.e., atmospheric turbulence), tracking error, pixel sampling, etc., and in the infinite limit, tends to a Gaussian function (cf. central limit theorem). The observed PSF encloses the remainder of the original source energy.

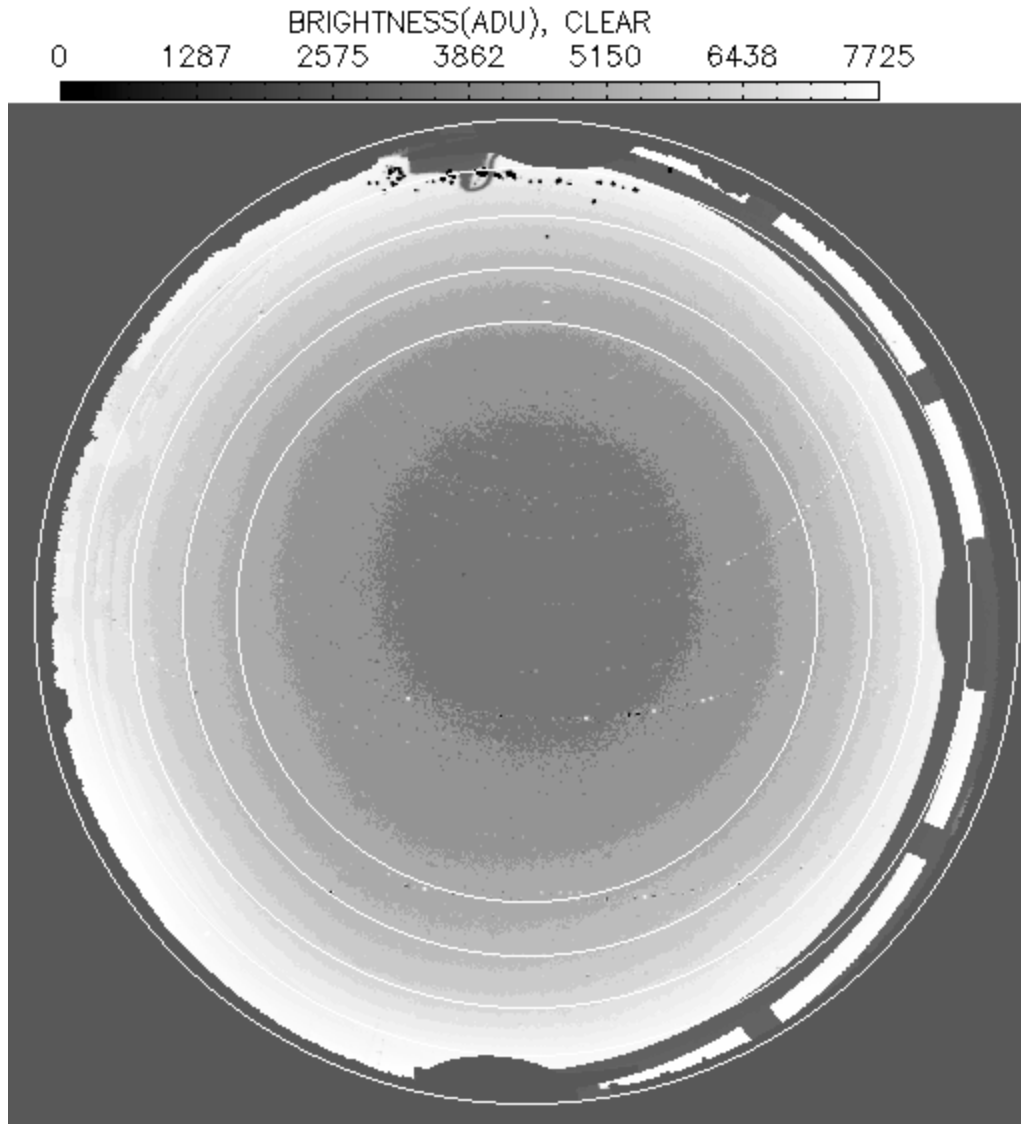


**Figure 6. Trails of non-completely subtracted stars, in an average over 60 frames are shown (Figure 6).** The contamination with other star's light is obvious when an elliptic aperture around a star is shown separately (Figure 7).

Moreover, besides optical system, the detection with a CCD introduces constraints of background-limited and separation-limited nature. For most but the brightest stars, the best Gaussian fit to the image gives a  $\text{FWHM} = 0.45 < 2\text{pixels}$  ( $\sigma < 0.85\text{pixels}$ ), i.e., spatially under-sampled. An amount of defocus was introduced by ARM in frames beginning in August 2002, to widen the image.

A point source can be represented by a Delta-Dirac function, and the optics has a specific PSF given by diffraction with aberrations; the constant-declination star trail on a projected conical trajectory produces a "Trail PSF", dependent on the position on the CCD, which gives an E-W curvature and a N-S shift, and the pixel is sampling the image with a sensitivity given by a box function  $\Pi$  (in the ideal case of an



**Figure 7.** Trails of non-completely subtracted stars, in an average over 60 frames are shown (Figure 6). **The contamination with other star's light is obvious when an elliptic aperture around a star is shown separately (Figure 7).**

uniformly sensitive pixel), and the electronics produces a noise. Symbol “\*” signifies convolution. In reality, the pixel function is very different from a box function, due to the differential absorption in the dielectric and in the metallic conductor layers built on the surface of a front-illuminated pixel.

### **Each Supplementary Feature Implied by WSI Measurements is Discussed Below**

**Crowded field and poor spatial separation.** The presence of many sources within a small area on the detector is the main cause of difficulty in obtaining a good empirical PSF profile. The radial angular resolution is 0.33deg/pixel at zenith and decreases to 0.43deg/pixel at the horizon. For aperture photometry, it is clear that one is looking not at a single source, but at entire patches of sky, with many sources in the same element of solid angle. While the optical depth computation is possible, the attribution of an exclusive color to the observed sky portion becomes a challenge.

**Tilt.** Optical axis in the local meridian plane and horizontal CCD slightly tilted with respect to the N-S direction: Before attempting to construct a PSF model, one should check for CCD alignment with the zenith and N-S direction. This makes a difference in the PSF shape and orientation. In this case, the CCD is not centered on the optical axis (Figure 8), and the radial distance with respect to the center of the CCD maps linearly the zenithal angle of the object. There is a very small angle of misalignment between N-S direction and N-S oriented columns of the CCD (Figure 9, left). The effect of this sampling on the Azimuth zero line (i.e., the North direction) is to make it look “segmented” (Figure 9, right).

**Trails.** Stars motion in the field of view: The PSF profile is smeared on a few neighboring pixels, due to the star (apparent) motion during the exposure time (this approaches the time-delayed-integration detection mode in astronomy, and also the “dithering” method for stacking astronomical images). Figure 10 presents the constant declination conical trajectories described by centers of the visible stars

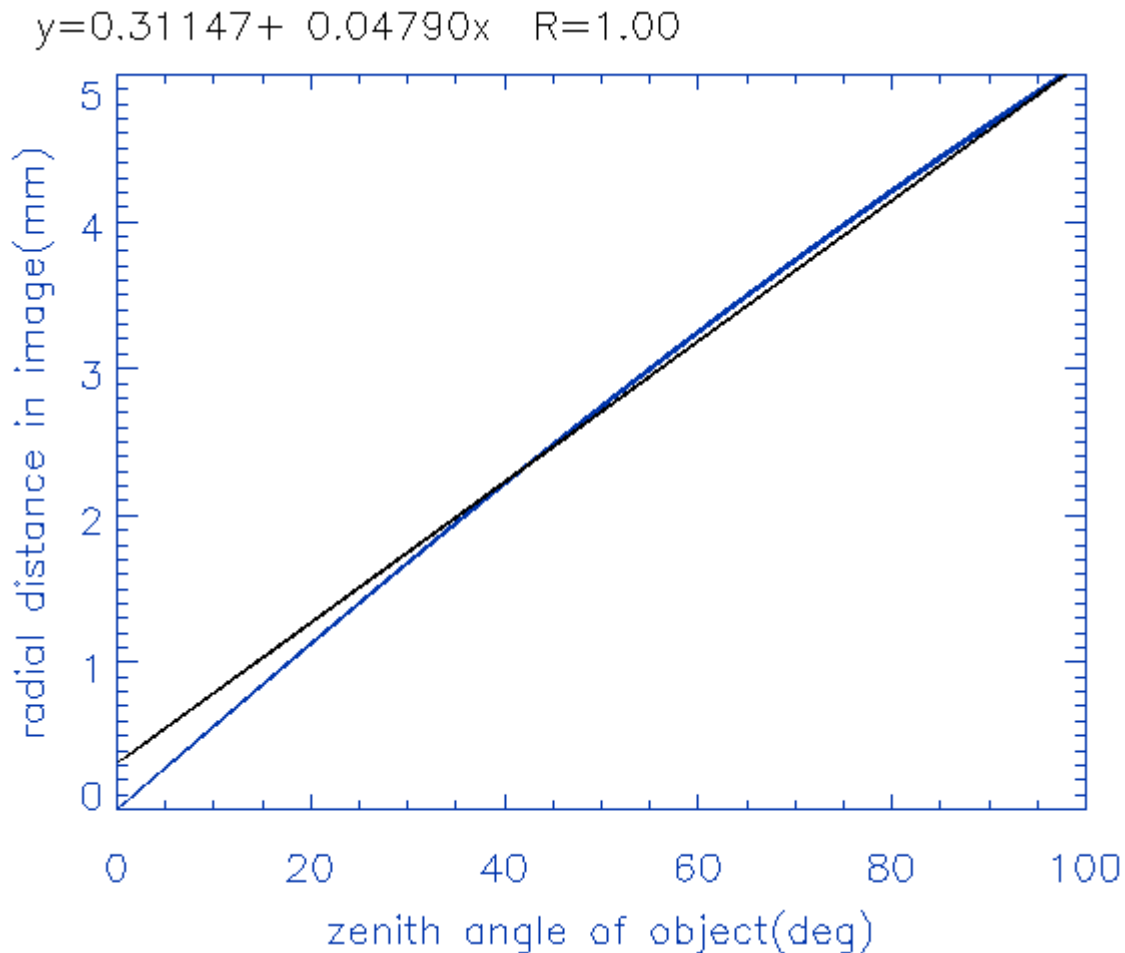


**Figure 8. Optical axis in the local meridian plane and horizontal CCD slightly tilted with respect to the N-S direction: The CCD is not centered on the optical axis (Figure 8), and the radial distance with respect to the center of the CCD maps linearly the zenith angle of the object.** There is a very small angle of misalignment between N-S direction and N-S oriented columns of the CCD (Figure 9, left). The effect of this sampling on the azimuth zero line (i.e., the north direction) is to make it look “segmented” (Figure 9, right).

during a 12 hours night, sampled during 1 minute at every 6 minutes, and Figure 11 shows 3 minutes integration over 3 pixels radius disks, in apparent motion (the night of 19990223). On a circle of constant declination, a small distance covered during 1 minute integration is proportional with the cosine of the declination:

$$\text{Length of trajectory (radians)} = \text{Hour angle variation (radians)} * \cos(\text{declination})$$

From this simulation one can infer that a 2D Gaussian with a width not aligned with columns and rows directions is suitable. This rotation angle should be one of the parameters of the PSF fit.

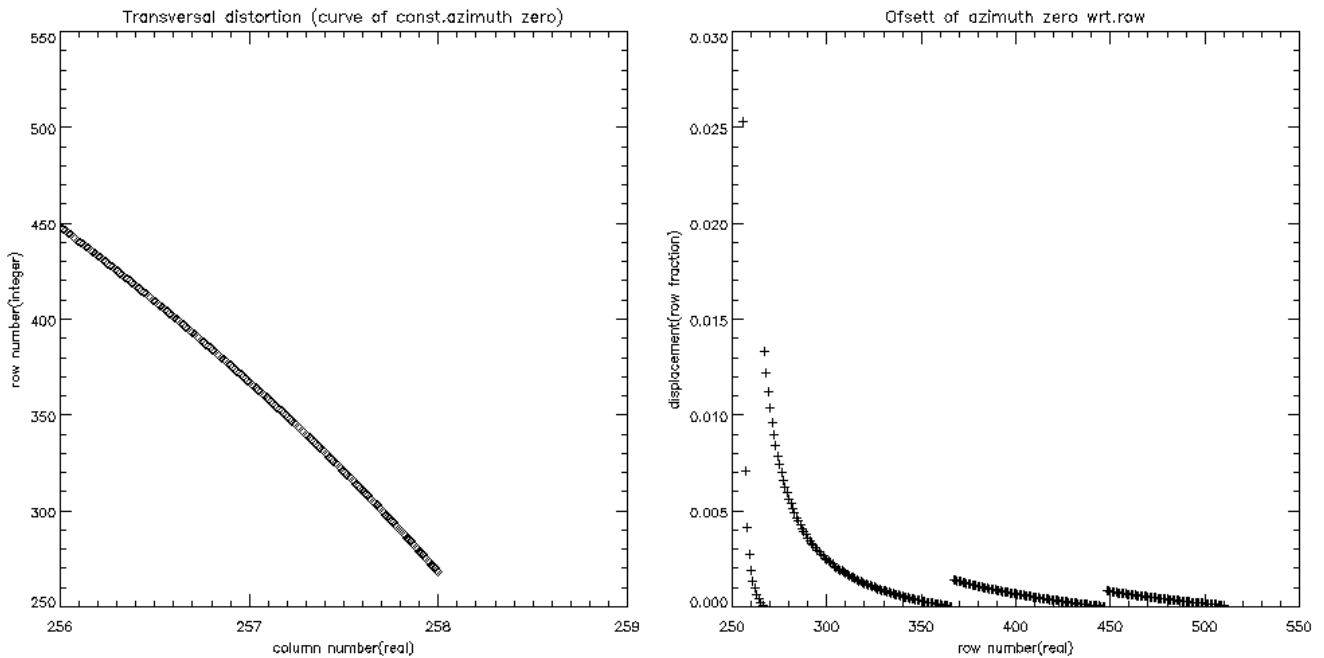


**Figure 9.** Optical axis in the local meridian plane and horizontal CCD slightly tilted with respect to the N-S direction: The CCD is not centered on the optical axis (Figure 8), and the radial distance with respect to the center of the CCD maps linearly the zenithal angle of the object. **There is a very small angle of misalignment between N-S direction and N-S oriented columns of the CCD (Figure 9, left).** The effect of this sampling on the azimuth zero line (i.e., the north direction) is to make it look “segmented” (Figure 9, right).

**Distortion and high sky gradient.** Regardless of the method one chooses to perform the photometry, one must first solve the complexity of flat fielding. There is a complicated, non-flat “sky” surface omnipresent in the field of view, due to the competing effects of vignetting (dropping in light input from center to margin in the lens, due to optical system stops) and barrel distortion (same radiance amount is distributed over areas which are decreasing from the center towards the edges of the FOV). Regarding the decrease of angular resolution at high zenith, and correspondingly, the enhancement of the sky brightness per pixel, a “flat” frame can be obtained by star subtraction and frame averaging for a uniform sky gradient configuration, where the North Galactic Pole is near the zenith (again, Figures 4 and 5). Another method of compensating for radial sky gradients is to choose an elliptical aperture with the large axis perpendicular on the radial distance in the image (again, Figure 7), mainly for zenith angles greater than 60 deg. Regarding the vignetting, Kumler and Bauer (2000) found that the relative illumination drops only to 80% at 80deg zenith, with respect to the illumination on the optical axis.

**Brightness range.** Several classes of objects are detected in a frame (Figure 12): in the upper bins there are brightest stars/planets and some cosmic rays spots, followed by fainter stars, diffuse “sky” and mask pixels in the lower bins.

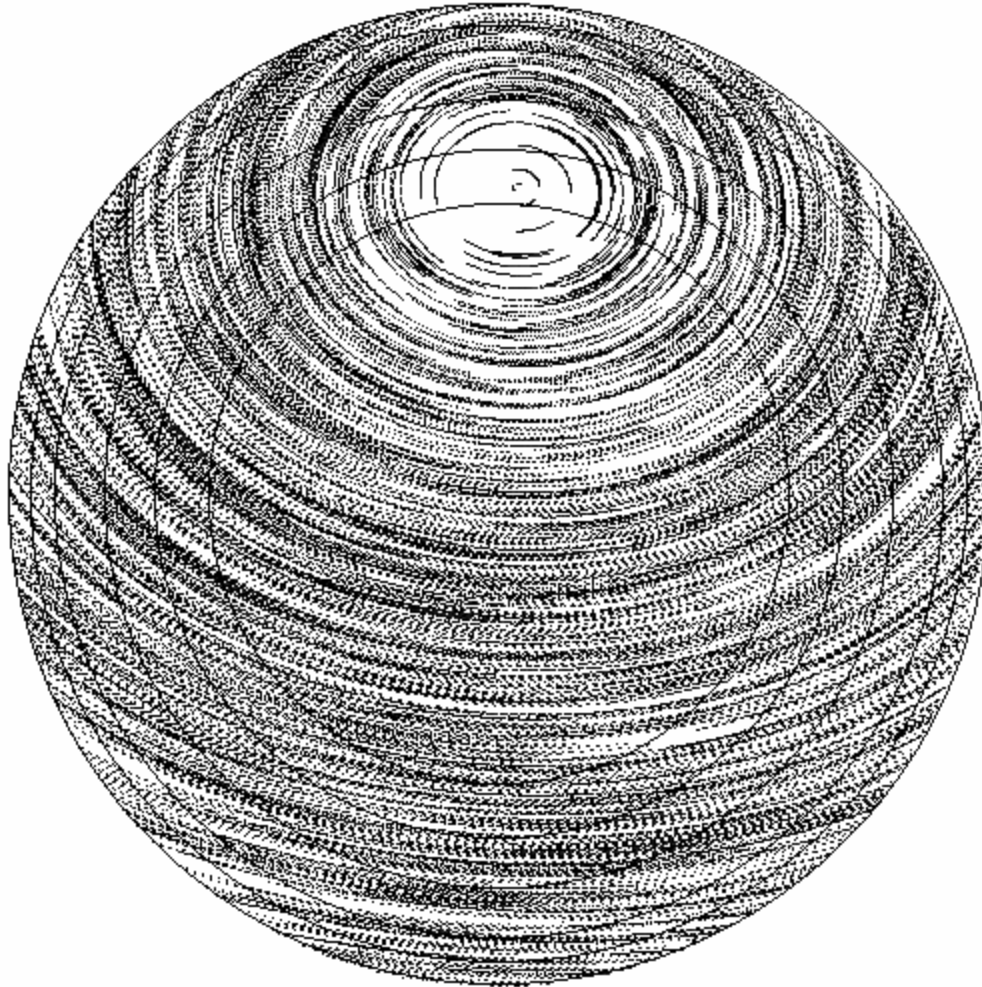


**Figure 10. Constant declination conical trajectories described by centers of the visible stars during a 12 hours night, sampled during 1 minute at every 6 minutes (Figure 10); and the 3 minutes integration over 3 pixels radius disks, in apparent motion, for the night of 19990223 (Figure 11).**

**Profile fitting** (on flattened frames). A star image has a central part of approx. the Gaussian shape (S). The flattened “sky” usually is a plane (B), but in WSI flat-subtracted frames it has a residual radial gradient. This small gradient is mainly due to the curvature difference between the multiple-frame averaged comparison profile (Figure 13) and the current frame. Intensity in a star pixel is an integral over one pixel of the model:

$$I(x_i, y_j) \equiv b_0 + b_1 x + b_2 y + A \int_{i-0.5}^{i+0.5} \int_{j-0.5}^{j+0.5} \exp(-[x'^2 / 2\sigma_x^2 + y'^2 / 2\sigma_y^2])$$

$$\begin{pmatrix} x' \\ y' \end{pmatrix} = R_\alpha \begin{pmatrix} x - x_0 \\ y - y_0 \end{pmatrix}, \alpha \text{ rot. angle}$$

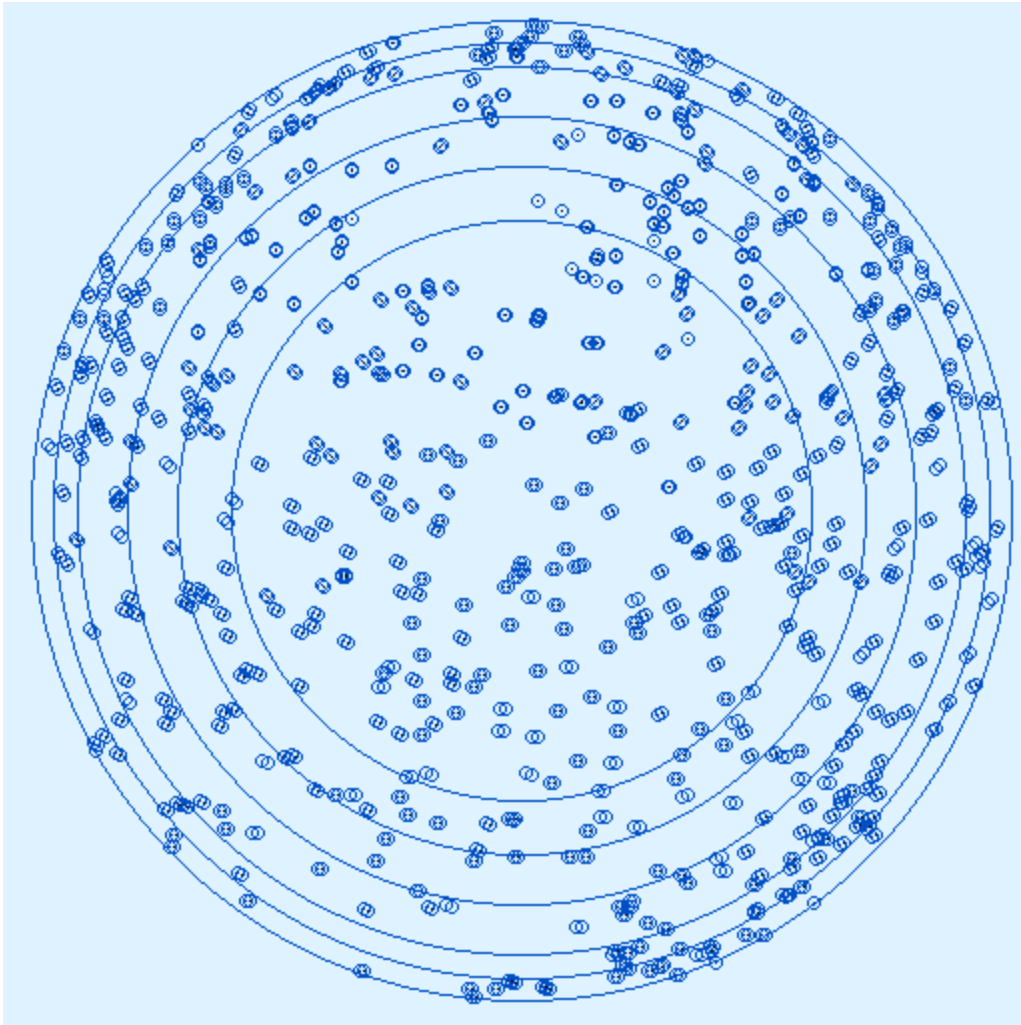


**Figure 11.** Constant declination conical trajectories described by centers of the visible stars during a 12 hours night, sampled during 1 minute at every 6 minutes (Figure 10); and **the 3 minutes integration over 3 pixels radius disks, in apparent motion, for the night of 19990223 (Figure 11).**

A non-linear least squares fit is performed. Star parameters to be fitted are the height of the Gaussian, FWHM on  $x'$ ,  $y'$  directions,  $\alpha$  rotation angle between the ellipse' axes and  $(x,y)$  coordinates, and the distance between the star image centroid and the center of the Gaussian.  $R\alpha$  is the rotation matrix.

$$\chi^2(A, \sigma_x, \sigma_y, \alpha, \Delta x_{CEN}, \Delta y_{CEN}) = \sum_1^N \frac{[I - (B + S)]^2}{\sigma^2} = \min.$$

The chi-square function minimization is done by adjusting, in small steps, a control factor in a set of linear PDE equations in first order derivatives of the S to the fitting parameters, until a convergence is achieved.

20000208.040600 clear 60sec; unit=1mWm<sup>-2</sup>sr<sup>-1</sup>nm<sup>-1</sup>

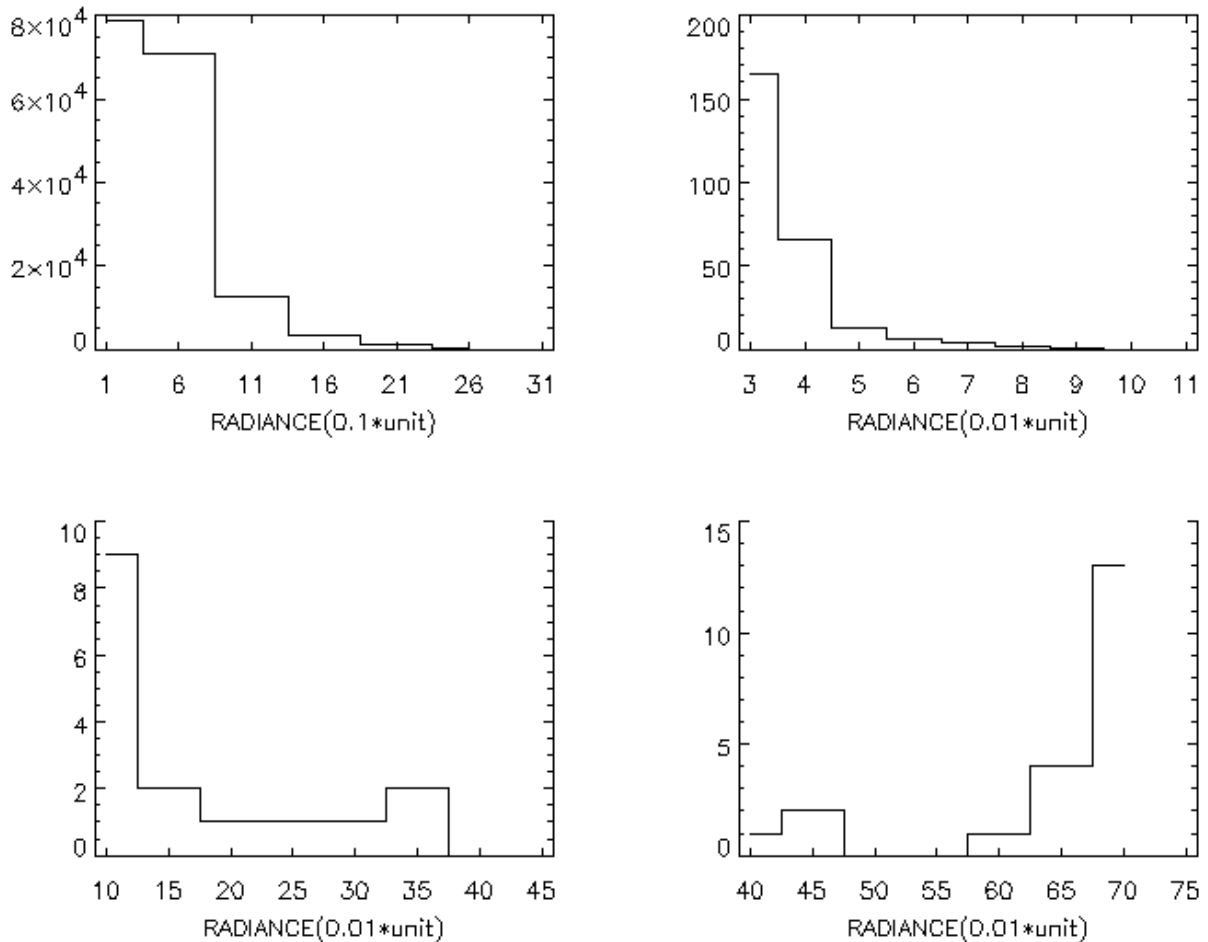


**Figure 12.** Sample histogram of visible sky radiance for 20000208.040600, broadband, 60 sec. Exposure time; in the upper bins there are brightest stars/planets and some cosmic rays spots, followed by fainter stars, diffuse “sky” and mask pixels in the lower bins.

The best fit is obtained in the form of Gaussian plus a residual matrix, which is stored with a double resolution. The unitary volume Gaussian has the advantage of being easy to integrate over the surface of a pixel, while the derivatives can be precisely computed. The fitted profile is shifted across the image to the location of the rest of the stars (non PSF stars) then it is scaled to their intensity and the volume (i.e., the magnitudes) for the respective stars is determined.

The linearity and invariance to the shifting in the optic field is a condition for simplifying the convolution computation as a sum and a product: it is the integral over pixels of a product of two functions, one being shifted across the CCD.

If the PSF is found to vary across the image (variable kernel), the FOV should be partitioned in areas of constant kernel.

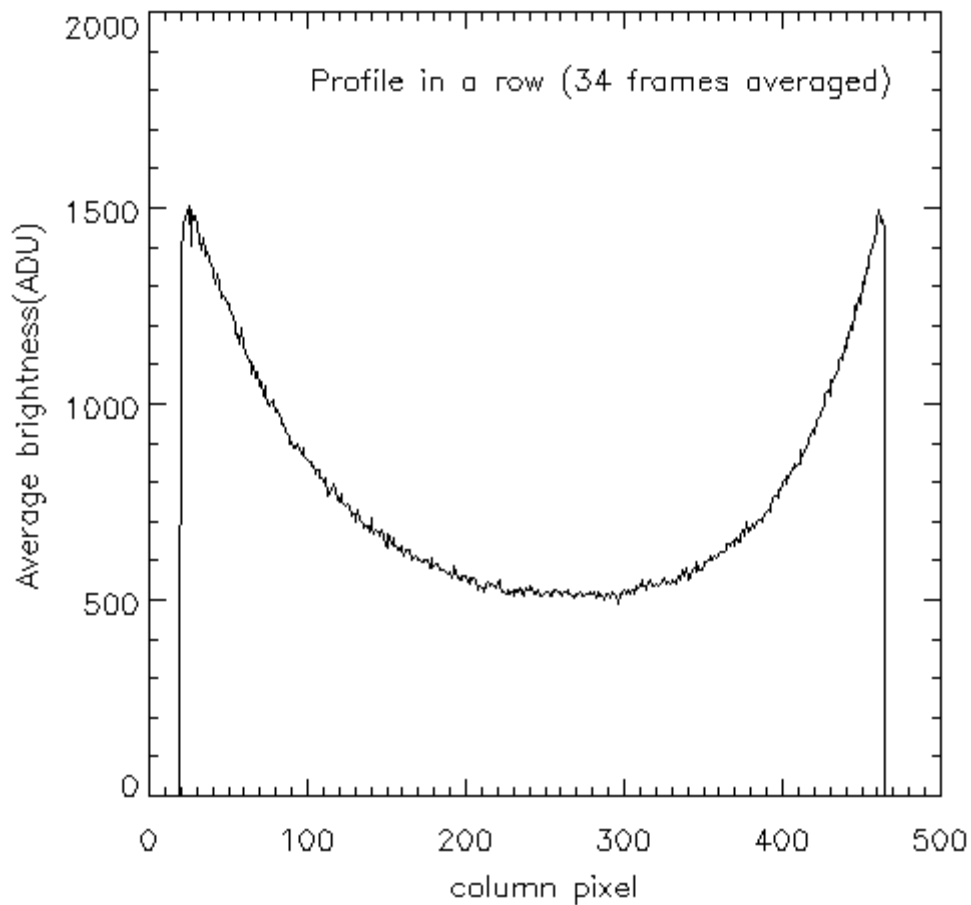


**Figure 13.** A transect through an average of many star-subtracted frames. The intrinsic (electronic) inter-pixel variance remains, while the sky component of the pixel-to-pixel variance was smoothed out.

Composite, constant-kernel PSFs for two frames are presented in Figures 14 and 15. It is obvious that a Gaussian does not correctly represent the star PSF, as imagined by the WSI.

Residuals significance: for unresolved stars, the residual matrix contains the best part of the signal, as the Gaussian is a poor fit. They also may contain the information on diffraction on the CCD grid. Mighell (2003) suggested that a way to recover the Nyquist sampling frequency from under-sampled data is to renounce altogether to the Gaussian function and use directly a “digitized” (matrix) PSF, with twice the resolution of the image. This deconvolution procedure will use first derivatives in parameters too, but they will be numerically computed.

**Comparison of results for aperture and profile fitting photometry with WSI images.** Extinction curve examples for circular aperture (“1”), elliptical aperture (“2”) and profile fitting photometry (“3”) are presented in Figures 16, 17, 18, and 19, for stars Capella, Aldebaran, Gamma Geminorum, and Vega, respectively. Accuracy is slightly improved when using the last.

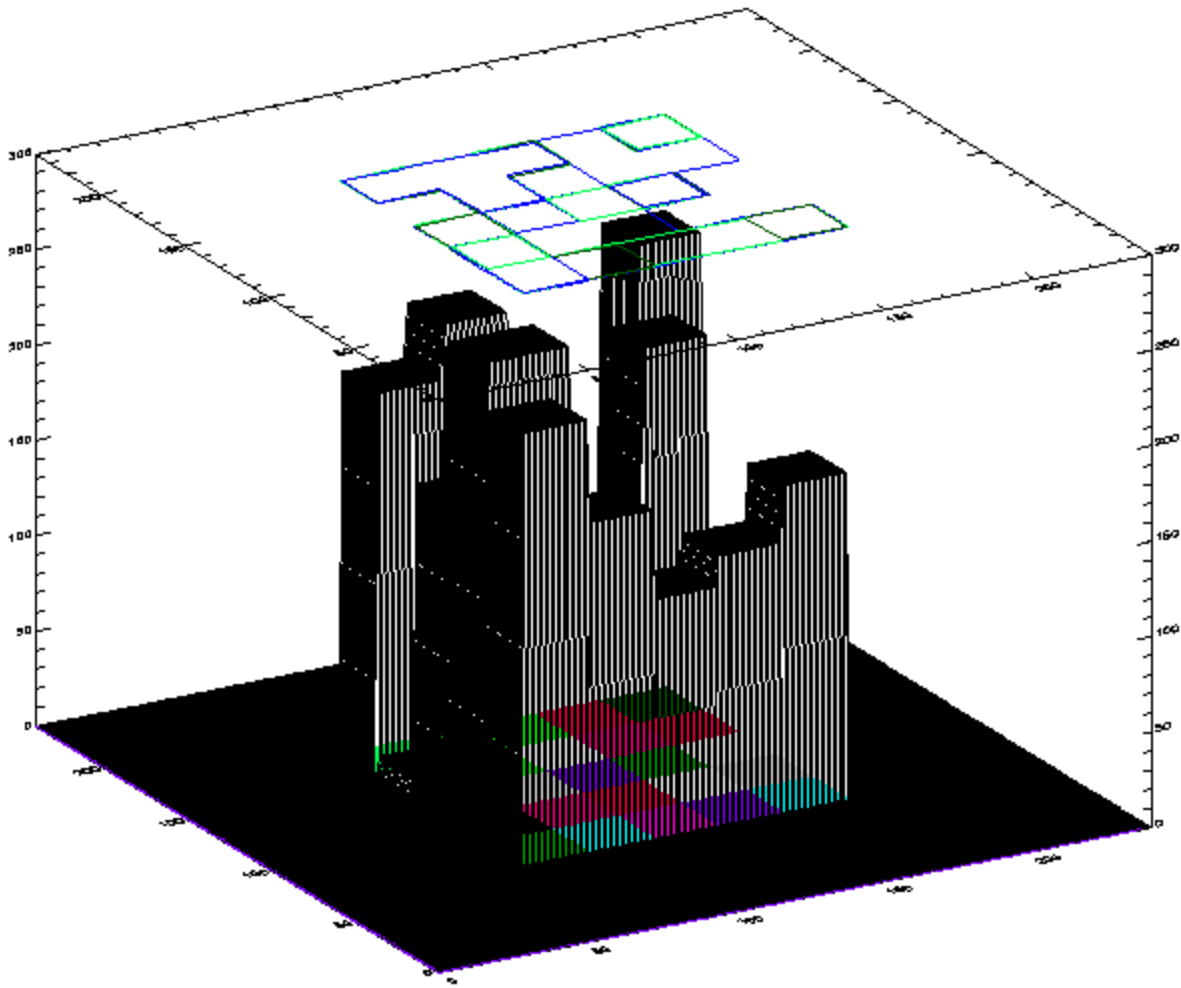


**Figure 14.** Actual PSF in two frames (20000208 and 19980119), magnified (a block represents a pixel). It is obvious that a Gaussian does not correctly represent the star PSF, as imagined by the WSI.

From the ratio of the errors in flux measured (Figure 20), one can see that the fitting and simple aperture are comparable in accuracy for most of the stars, with fitting performing slightly better. Fitting does include the aperture procedure, but on a smaller area, thus contamination from other stars in the background near the program star is lowered.

**Extinction measurements.** Usually, astronomers observe 4 stars at two air-masses each, for zenith angles less than 60deg., relative air-mass = 2. We were able to observe to up to 85deg., 200 stars with S/N = 100...1000, and the flux values reduced with profile fitting show a remarkable low dispersion with respect to the mean. Considering that the quantum efficiency has a maximum sensitivity in red (effective wavelength around 680nm), one can compute a value for Rayleigh extinction for the altitude  $h$  (m) of the observing site:

$$k_R \cong 0.107 \times \left(\frac{\lambda_{\text{eff}}}{550}\right)^{-4} e^{(-h/7996)} \approx 0.044,$$

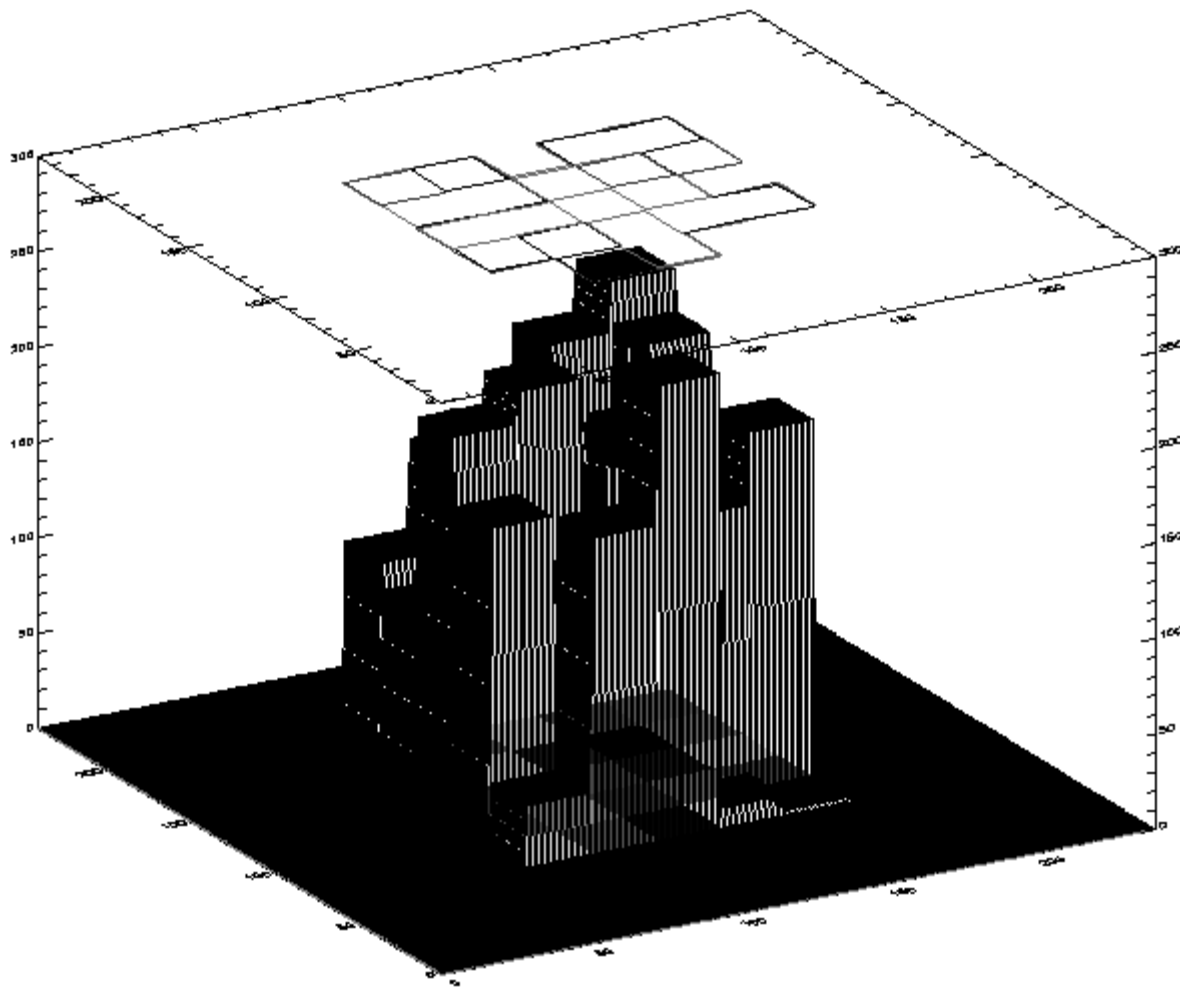


**Figure 15.** Actual PSF in two frames (20000208 and 19980119), magnified (a block represents a pixel). It is obvious that a Gaussian does not correctly represent the star PSF, as imagined by the WSI.

Above the site, the O<sub>3</sub> amount corresponding to each of the below listed days (306, 363, and 261 DU, respectively) does not display a variation correlated with the calculated “residual extinction.” Residual extinction in the Table 1 is thus an indication of the aerosol content in the atmosphere.

<b>Table 1.</b> Extinction measurements (see text).				
<b>Number Frames Reduced</b>	<b>Number Stars used; Maximum Zenith</b>	<b>Mean Extinction (mag/airmass)</b>	<b>Error in the Mean</b>	<b>Residual Extinction (mag/airmass)</b>
110 (12021999)	36; 76deg.	0.120	0.010	0.076
39 (23021999)	19; 75deg.	0.149	0.012	0.105
50 (27102001)	27; 75deg.	0.157	0.011	0.113

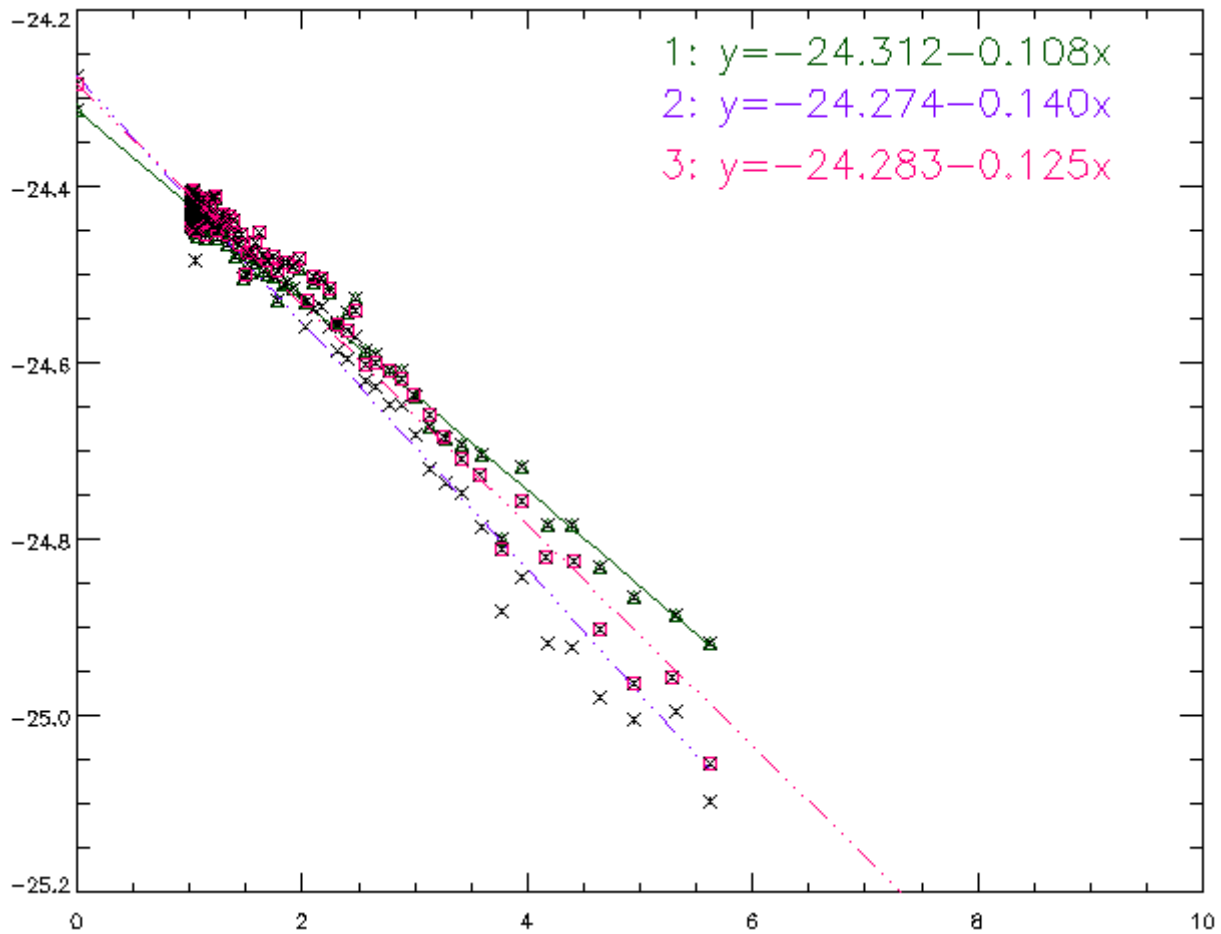


**Figure 16.** Extinction-curve examples for circular aperture (“1”), elliptical aperture (“2”) and profile fitting photometry (“3”), for stars Capella, Aldebaran, Gamma Geminorum, and Vega, respectively.

## Conclusion

The reduction of star flux frames obtained with the WSI can be improved when adopting a suitable model for the PSF stars. The principal benefit is obtaining improved flats in clear nights. Consequently, the ability to measure small variations in residual extinction (due mainly to aerosols) will be improved. This is a work in progress.

## Corresponding Author

Ileana C. Musat, [musat@atmos.umd.edu](mailto:musat@atmos.umd.edu), (301) 405-5348

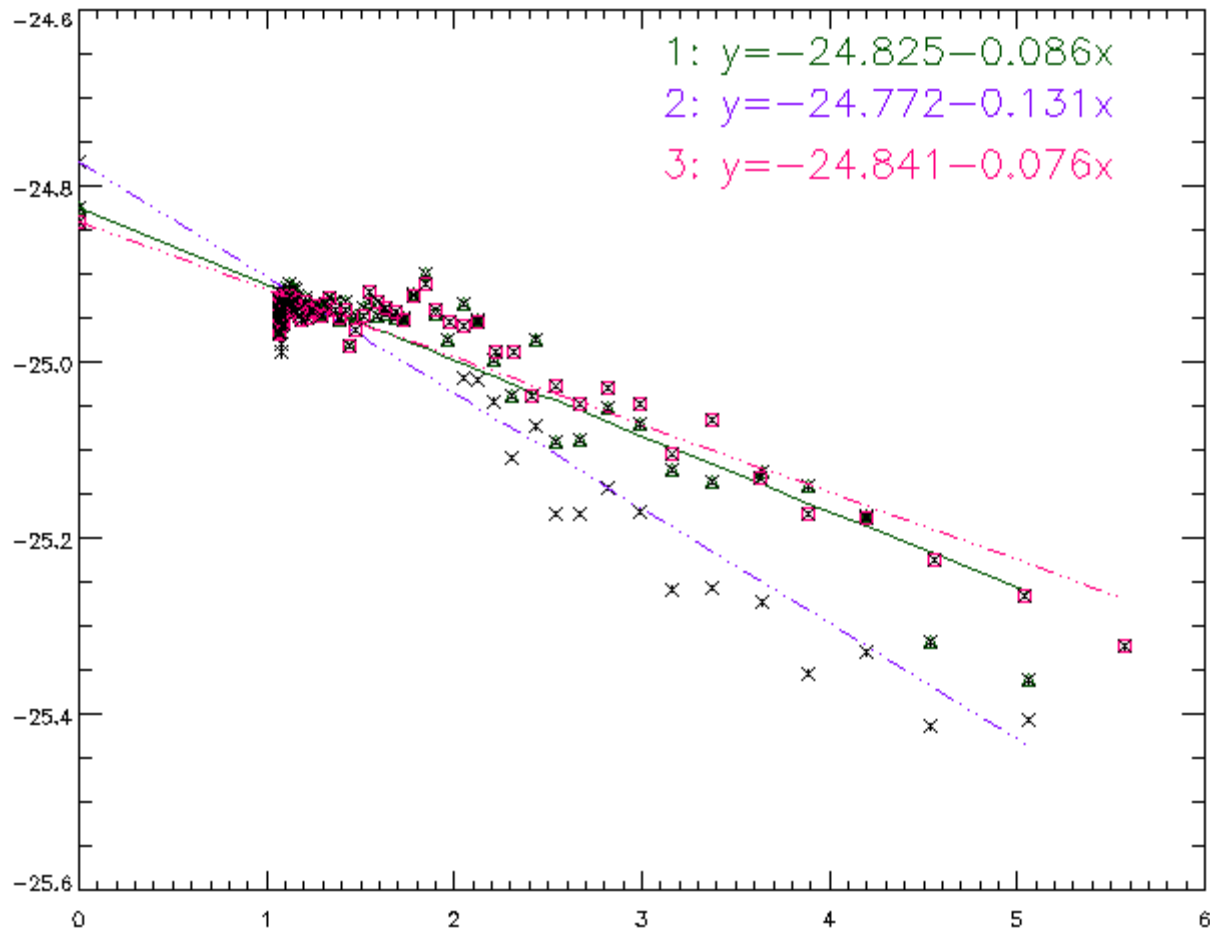


**Figure 17.** Extinction-curve examples for circular aperture (“1”), elliptical aperture (“2”) and profile fitting photometry (“3”), for stars Capella, Aldebaran, Gamma Geminorum, and Vega, respectively.

## References

Kumler, J. J., 2000: Martin Bauer, Fisheye lens designs and their relative performance. *Proc. SPIE*, Vol. 4093, pp.360-369.

Mighell, K. J., 2003: Astronomical Data Analysis Software XII ASP Conference Series, Vol. 295, p.395.

Stetson, P. B., 1987: Daophot: A computer program for crowded field stellar photometry, *Pub.Astron.Soc.Pacific*, **99**, pp.191-222.

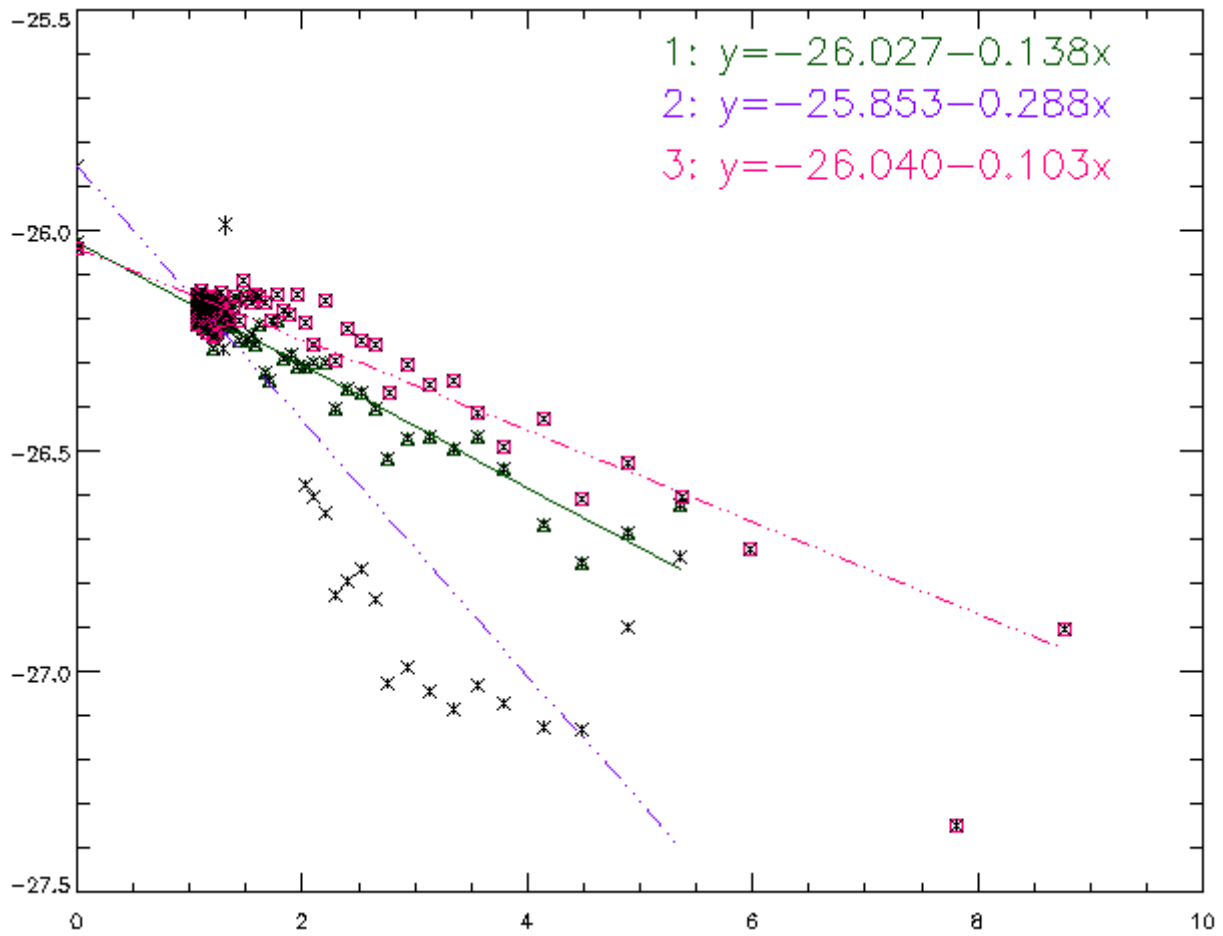


**Figure 18.** Extinction-curve examples for circular aperture (“1”), elliptical aperture (“2”) and profile fitting photometry (“3”), for stars Capella, Aldebaran, Gamma Geminorum, and Vega, respectively.

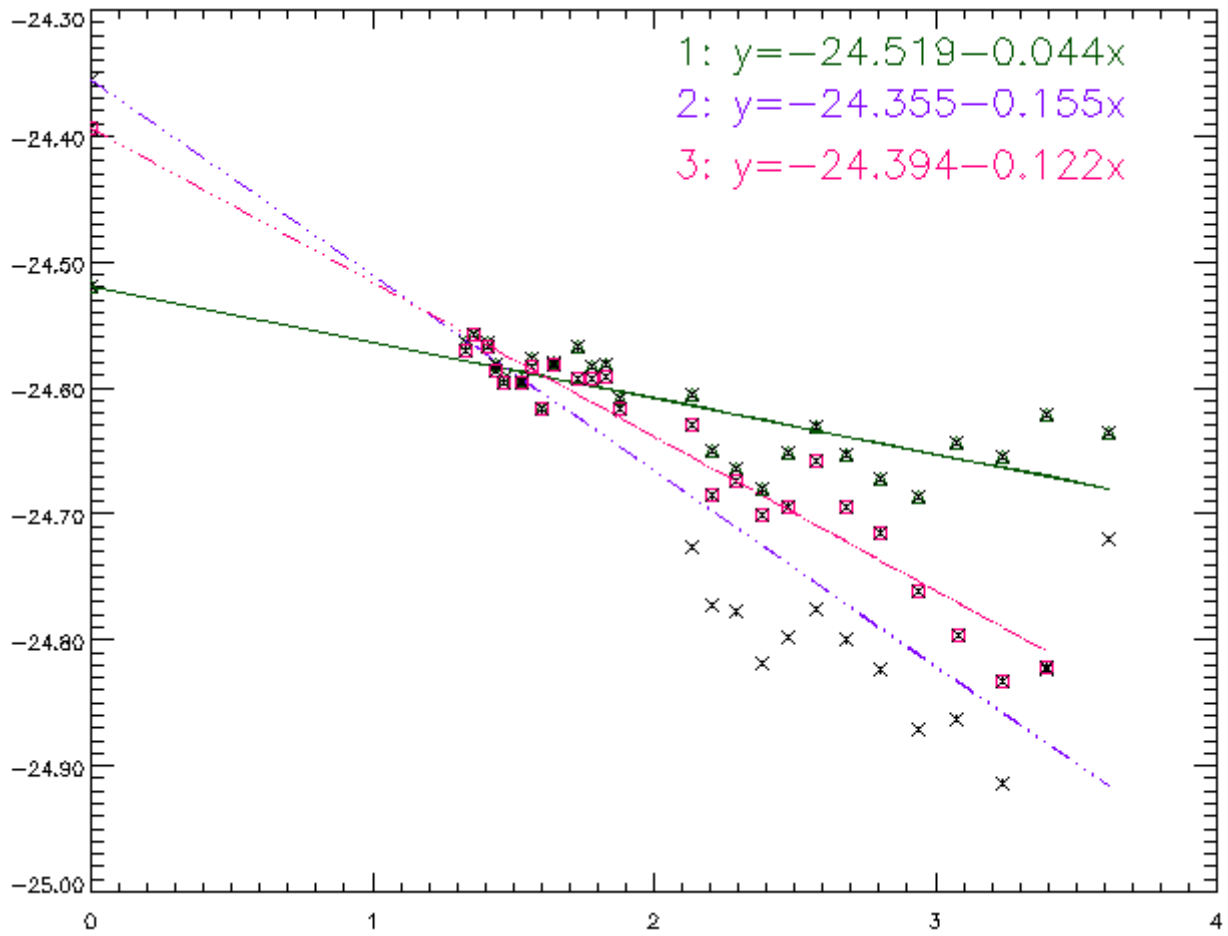


**Figure 19.** Extinction-curve examples for circular aperture (“1”), elliptical aperture (“2”) and profile fitting photometry (“3”), for stars Capella, Aldebaran, Gamma Geminorum, and Vega, respectively.

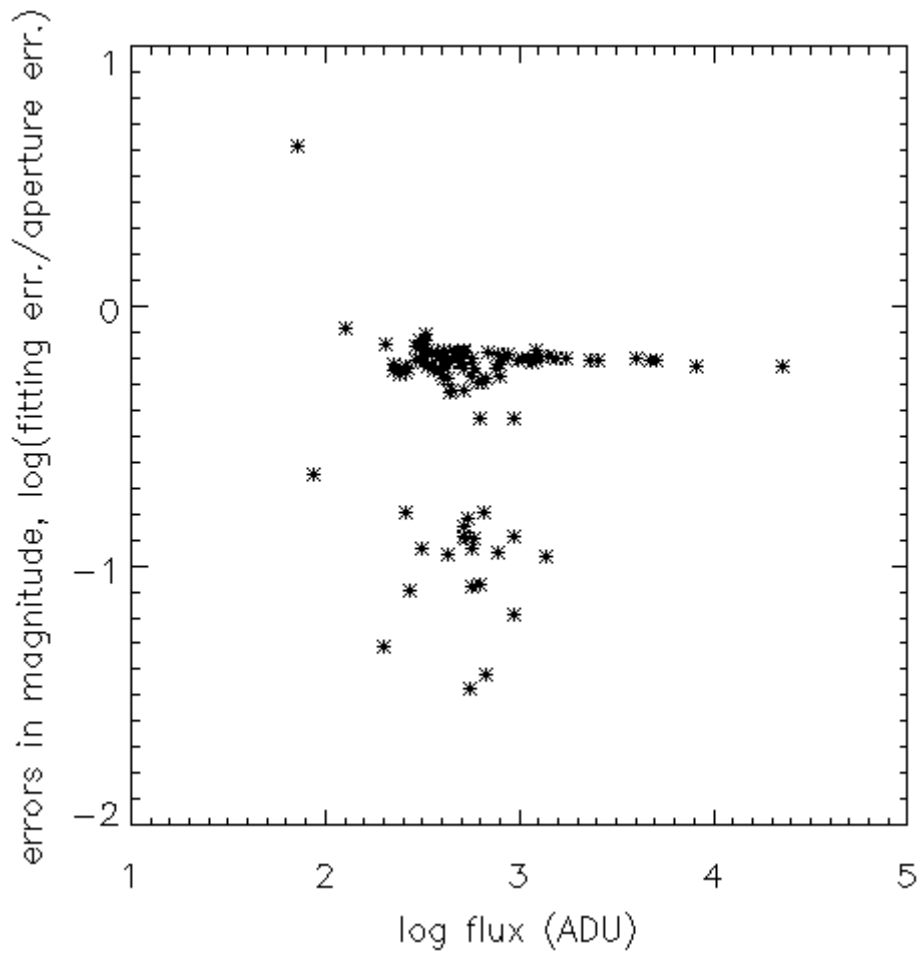


**Figure 20.** The ratios of error in star magnitude calculated through fitting method and through aperture method, versus flux values (Figure 20). Equivalently, the signal-to-noise ratio for fitting on sky-  
"flattened" frames is slightly better than that for aperture method.